Tellus (1998), 50A, 124–133
Printed in UK – all rights reserved

TELLUS
ISSN 0280–6495

Sensitivity of a coarse resolution ocean general circulation model under climate change forcing

By WILLIAM A. GOUGH* and TATIANA ALLAKHVERDOVA, *Environmental Science, Physical Sciences Division, University of Toronto at Scarborough, 1265 Military Trail, Scarborough, Ontario M1C 1A4, Canada*

(Manuscript received 23 May 1997; in final form 30 September 1997)

ABSTRACT

Tunable parameters in an ocean general circulation model are assessed as modifiers to the model response to several climate change scenarios. For the current climate scenario it is found that vertical diffusivity plays a dominant rôle as expected. An analysis of the horizontal diffusivity variation suggests that use of the peak value of the overturning streamfunction is a misleading indicator of model flow strength. For the warming and cooling scenarios vertical and horizontal diffusivity variations dominated the equilibria response. However, these tunable parameters are of minor significance in the transient response in the cooling scenarios. The diffusively dominant warming scenarios, in contrast, very much depend on the magnitude of the vertical diffusivity. This has important implications for the use of coarse resolution models in coupled atmosphere-ocean model climate change simulations.

1. Introduction

Coarse resolution ocean general circulation models are commonly used in climate change scenario simulations (Kattenberg et al., 1996). These models are dependent on tunable parameters used to approximate sub-grid scale processes. It is of interest to assess model parameter sensitivity in the model's response to typical climate change scenarios.

Coarse resolution models ($>1^\circ$) are not capable of resolving mesoscale eddies, salt fingering, double diffusion, internal breaking waves, and convection. Mesoscale eddies mix laterally and have traditionally been represented by horizontal diffusion. More recently isopycnal mixing has been used to more accurately represent mesoscale eddies (Veronis, 1975; McDougall and Church, 1985; Gough and Welch, 1994; Danabasoglu et al., 1994; Gent et al., 1995). This has improved the representation of CFC uptake (England, 1995; Robitaille and Weaver, 1995). It has also mitigated the Veronis effect — the anomalous interior downwelling resulting from cross isopycnal mixing (Gough and Lin, 1995). Sarmiento (1983) and Toggweiler et al. (1989) speculated that using isopycnal mixing would improve passive tracer distribution.

Salt fingering, double diffusion and internal breaking waves cause the vertical mixing of temperature, salt and other ocean tracers. This has been represented as vertical or diapycnal diffusion. Convection occurs when vertical columns of sea water become statically unstable. A number of methods have been devised to remove this instability (see Gough, 1997 and references therein). Bryan (1987) found that the magnitude of the vertical diffusivity was a crucial parameter which dictates the strength of the meridional overturning, the northward heat transport and the depth of the thermocline. Large values of the horizontal diffusivity have been associated the Veronis effect (Gough and Welch, 1994; Gough and Lin, 1995).

* Corresponding author.

In the above discussion three processes in the ocean are mentioned: diffusion, convection and advection. Each of these processes operate on different time scales. Diffusion typically operates on millennial timescales. For example, using the canonical value of 1 cm^2/s for the diffusivity for a 4000 m depth ocean yields a time scale of 5000 years. In contrast convection operates on a time scale of less than one year. Typically convection is treated as intense vertical diffusion with a diffusivity ranging from 10^4–10^5 cm^2/s. For a 4000 m deep ocean this leads to a time scale ranging from 1 month to half a year. The advective time scale for a basin such as the North Atlantic is typically centennial. For a 50° latitude basin with speeds approximate 0.1 cm/s, a time scale of 200 years is obtained.

The world's oceans act as a massive geochemical buffer for trace elements in the atmosphere. This buffering activity plays a crucial role in determining the atmospheric concentration of greenhouse gases. Up to 40% of anthropogenically released carbon dioxide, for example, is sequestered by the world oceans (Najjar, 1992). This, in turn, impacts on the potential amount of global warming that may occur in the climate system. It is therefore important to understand the process and time scale of tracer sequestering by the ocean, how this process may be modified during a period of climatic change, and how sensitive this uptake is to model parameterization.

Bryan et al. (1984) examined the impact of small warm and cold temperature anomalies at the surface of an ocean general circulation model on the ocean circulation. They noted changes in the ocean circulation and the relative rates at which the anomaly was assimilated by the ocean. The cold anomaly produced an immediate intensification of the flow and a more rapid uptake of tracer. A long term response was not investigated. Gough and Lin (1992) found strikingly different behaviour for the ocean's transient and equilibrium responses to warming and cooling anomalies. A cooling anomaly produced, in the short term, an intensified flow as was found in Bryan et al. (1984). The equilibrium response, however, was that of a weaker flow. The warming case produced the opposite results. They concluded that the transient response was dictated by the initial conditions when the anomaly was imposed while the equilibrium response was attributed to the new upper boundary condition, i.e. the surface density gradient resulting from the restoring temperatures and salinities. Qualitatively similar results were found in Bryan and Spelman (1985).

The IPCC report (Kattenberg et al., 1996) provides us with usable estimates of future temperature change. The most recent estimate is a warming of 1.0°C to 3.5°C by 2100. This is a globally averaged value and is lower than the 1990 estimate (Houghton et al., 1990) primarily due to the inclusion of sulphate aerosols in the atmosphere component of coupled models. The climate change scenarios in this work are loosely based on these predictions. We note though that we consider only thermal changes. There is the potential for substantial changes to the fresh water and momentum fluxes into the ocean as well and this is not considered here.

In this work we contrast the impact of varying model parameters such as vertical and horizontal diffusivity to the impact of changing the thermal boundary condition with current global warming estimates on the model flow and the uptake of a passive tracer. First, as a benchmark, we examine tracer uptake during the "current" climate. Here we find that the use of a traditional measure of the ocean flow, the peak value of the vertical overturning streamfunction, may be misleading and we propose alternatives. Second we examine the uptake of passive tracer under various climate scenarios and various values of horizontal and vertical diffusivity. It is found that although tracer uptake is clearly dependent on temperature change scenario, it is more sensitive to variations in the vertical diffusivity for the equilibrium response and plays a significant role in the transient response to a warming scenario. However, variations in vertical diffusivity play only a minor role in the transient response to a cooling scenario.

2. Model and experiments

2.1. Model

2.1.1. Governing equations. The model used in this work is the widely distributed Bryan-Cox ocean general circulation model. It is based on the pioneering work of Bryan (1969). A detailed description of the model can found elsewhere (Cox, 1984; Pacanowski et al., 1991). The notation used is standard.

2.1.2. Boundary conditions. In this model the only source of heat (temperature) and salinity forcing is at the upper surface. Therefore, at the side walls and bottom, a no-flux condition is imposed.

For the vertical side walls there is a no-slip (u, $v=0$) condition. At the bottom boundary, the flow is constrained to be parallel to the bottom topography, $w=0$, in the case of this model with a flat bottom. The condition on u and v is determined by the imposed bottom friction,

$$\tau_\lambda = \rho_0 C_D (u^2+v^2)(u\cos\alpha - v\sin\alpha), \quad (1)$$

$$\tau_\phi = \rho_0 C_D (u^2+v^2)(u\sin\alpha - v\cos\alpha), \quad (2)$$

where C_D, the drag coefficient, is 1.3×10^{-3} and α, the turning angle is -10° for this study. For the vertical velocity, the rigid lid approximation is used ($w=0$ at $z=0$).

The horizontal momentum, at the upper surface, is forced by the atmospheric winds. This is accomplished by using idealized wind stresses (τ_λ, τ_ϕ) given by the following analytic representation,

$$\tau_\lambda = 0.2\text{–}0.8\sin(6\phi), \quad (3)$$

$$\tau_\phi = 0.0, \quad (4)$$

with the wind stress in units of dynes/cm^2. This particular choice is designed to roughly reproduce the two gyre circulation in the North Atlantic, the approximate region of the model domain. The model has a $2^\circ\times2^\circ$ horizontal resolution extending from 20°N to 70°N and from 0–60°W. There are 10 vertical levels of increasing thickness, emphasizing the more active thermocline region (Table 1).

In this work restoring boundary conditions are used for both temperature and salinity (Haney, 1971). The restoring values are loosely based on the Levitus (1982) data set and are presented as eqs. (5) and (6) for temperature and salinity respectively.

$$T(\phi) = 27.0 - \frac{5}{9}(\phi - 20^\circ), \quad (5)$$

$$S(\phi) = 36.0 - \frac{1}{25}(\phi - 20^\circ), \quad (6)$$

where ϕ is the latitude and the temperature in Celsius and salinity in parts per thousand. The diffusion constant corresponds to a restoring timescale of 50 days for a 50 m upper layer.

The same restoring time scale is used for a passive tracer. Typically air-sea gas exchange is represented by a "piston velocity" (Najjar, 1992). The piston velocity is dependent on the ocean viscosity and diffusivity, the wind speed and ocean temperature. The actual uptake is further modified by the solubility of the geochemical. The piston velocity of CO_2, for example, has been estimated at 10 m/month. Converting the restoring time scale used in this model to a piston velocity yields 30 m/month representative of a less soluble tracer. Variations in the piston velocity as a function of temperature and wind speed have been ignored in this study in order to more clearly identify the dynamical processes (advection, convection, diffusion) involved in tracer uptake.

Table 1. *The vertical structure of the model*

Level	Depth (m)	Layer thickness (m)
1	25	50
2	75	50
3	150	100
4	300	200
5	500	200
6	750	300
7	1100	400
8	1650	700
9	2500	1000
10	3500	1000

Each level is located at the midpoint of the corresponding layer. The total ocean depth is 4000 m, the sum of the layer thickness.

2.2. Experiments

A series of 9 simulations are run in which the vertical eddy diffusivity, K_V, and horizontal eddy diffusivity, A_H, are varied. Three values of K_V are used (0.5, 1.0, 2.0 cm^2/s) and 3 values of A_H (1.0, 2.0, 5.0×10^7 cm^2/s). Both K_V and A_H are larger than can be justified from observations (Ledwell et al., 1993). K_V is large in order to produce a reasonable northward heat transport and depth of the thermocline. A_H is large in order to suppress numerical noise. These experiments serve to assess model sensitivity prior to imposing the climate change scenarios. The experiments are listed in Table 2 in the next section.

For the temperature change scenarios, three additional types of simulations are done, one

Table 2. *List of experiments and results of equilibria tracer experiments*

Case	Vertical diffusivity (cm^2/s)	Horizontal diffusivity (10^7 cm^2/s)	Overturning streamfunction a (Sv)	Overturning streamfunction b (Sv)	95% tracer equilibrium a (years)	95% tracer equilibrium b (years)	95% tracer equilibrium c (years)
1	0.5	1.0	11.36	4.83	631	617	664
2	1.0	1.0	13.93	6.63	476	458	499
3	2.0	1.0	17.19	9.52	341	334	354
4	0.5	2.0	11.95	5.63	548	540	565
5	1.0	2.0	14.84	7.59	424	416	443
6	2.0	2.0	19.16	10.86	316	313	332
7	0.5	5.0	9.94	5.50	503	497	541
8	1.0	5.0	13.04	7.82	394	377	412
9	2.0	5.0	17.82	11.72	276	274	290

For the overturning streamfunction, *a* designates the peak value and *b* designates the value at 45° and 1300 m. For the tracer equilibrium values, column (a) designates the regular climate, column (b) represents the two warming cases and column (c) the cooling case. Due to only minor variations, the two warming cases are represented by one value.

cooling and two warming cases. The warming scenarios consist of (1) a 3° warming of the surface restoring temperature everywhere and, (2) a latitudinally ramped warming spanning three to five degrees with the largest warming occurring near the pole. This is done to mimic the expected polar amplification of the warming. The cooling case is a reduction of the restoring temperatures by three degrees everywhere.

All cases are spun up from rest for 2000 years (Bryan, 1984). At this time tracer is introduced at the ocean surface. Assuming an infinite source of tracer in the atmosphere (as the simplest first order case), a restoring boundary condition is set for the tracer with a value of 10.0 tracer units. The efficiency of the tracer uptake can be measured by the time it takes for the ocean to fill with tracer. 95% full, for example, occurs when the basin average is 9.5.

3. Results and discussion

3.1. Equilibrium simulations for standard climate

3.1.1. Basin averaged tracer uptake. To assess how quickly the ocean model sequesters tracer, we examine the time it takes for the ocean to become 95% "full" of tracer, i.e. the time it takes to reach an average value of 9.5. This is presented in Table 2 in column "a". The time for this equilibration ranges from 276 years to 631 years, a centennial time scale indicating that advection is the dominant process for tracer uptake. The K_V dependency is seen by comparing the first three cases. The sequestering time drops as K_V increases. This is as expected. With a larger K_V, the model's circulation as measured by the peak value of the meridional and zonal overturning streamfunctions is more intense (Bryan, 1987) and leads to a more rapid transport of tracer to deeper levels through advection. The dependence on the horizontal eddy diffusivity is seen by comparing cases 2, 5 and 8. Here the vertical eddy diffusivity is held constant at 1.0 cm^2/s. The time to reach 95% of the equilibrium value does decrease with increasing horizontal eddy diffusivity but much less so than with vertical diffusivity.

Although the correlation between the peak value of the overturning streamfunction and the K_V dependence in the tracer uptake was clear, it is not so in the A_H case. The overturning streamfunction in Table 2 shows an increase as the horizontal diffusivity increases from 1.0×10^7 cm^2/s to 2.0×10^7 cm^2/s but decreases for the highest value of A_H. Even though the peak value was lower for this high values of A_H, the overturning as measured indirectly by the tracer uptake must have been stronger. The peak value of the meridional overturning streamfunction may not be the best representation of the overturning.

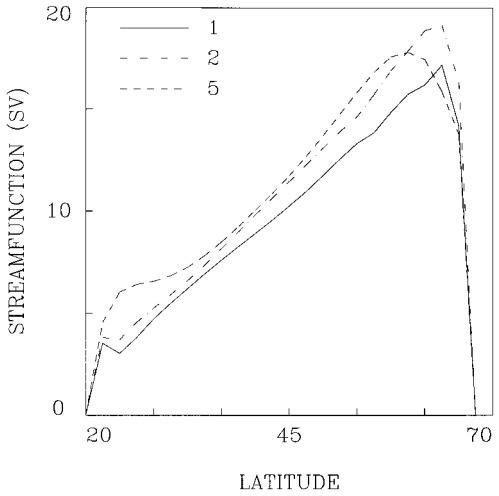

Fig. 1. Graph of peak value of the meridional overturning streamfunction as a function of latitude and horizontal diffusivity. Diffusivity is in units of 10^7 cm^2/s, overturning streamfunction in Sverdrups (1 Sv = 10^6 m^3/s). $K_v = 2.0$ cm^2/s for each case.

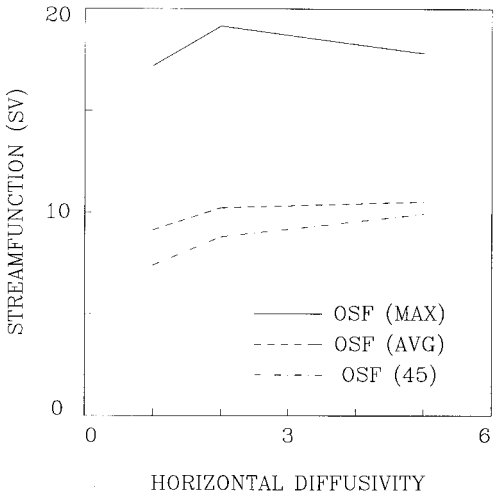

Fig. 2. Plot of three measures of the basin overturning flow: the peak value of the overturning streamfunction, OSF (MAX), the basin average of the overturning streamfunction, OSF (AVG), and the overturning streamfunction at 45° N, OSF (45). All are plotted as a function of the horizontal diffusivity measured in 10^7 cm^2/s.

We examine this issue further by plotting the maximum of the overturning streamfunction for each latitude. This is presented for the range of horizontal eddy diffusivities in Fig. 1 (cases 3, 6, and 9). From this it is clear that there are more sharply defined extrema for the lower values of A_H, while for the larger value there is a broader and less intense peak in the streamfunction value. Two further diagnostics are suggested by this analysis. The first is to select a median latitude that is less susceptible to the polar intensification of extrema as suggested by Winton (1996). The second is to average the streamfunction over the entire latitudinal range, essentially creating a measure of the basin flow strength. These two diagnostics as a function of the horizontal eddy diffusivity are presented with the corresponding curve for the peak value of the overturning streamfunction for the basin (i.e., isolating the northern extrema in Fig. 1). The two new diagnostics (Fig. 2) do not show a reduction in value for larger A_H values. This is consistent with the uptake analysis and supports the assertion that the use of the peak value of the meridional overturning streamfunction is potentially misleading even when advection dominates.

In Table 3 we continue this analysis by comparing power relationship between the strength of the overturning streamfunction and vertical diffusivity, i.e., $\mathrm{OSF} = aK_V^n$. The strength of the overturning is measured in two ways, the traditional peak value of overturning and the value of the overturning at 45° and 1300 m. The first diagnostic produces an n value similar to that found by Bryan (1987) and Winton (1996) of approximately 1/3. The second diagnostic produces a larger value of approximately 1/2 again consistent with Winton (1996) but less than the 2/3 predicted by scaling arguments. In the final two columns the 95% full time scale is similarly analyzed and produces an n value of approximately $-1/2$, the negative sign signifying a decreasing time for larger values of K_V. This further confirms the dominant role that vertical diffusivity has in the determination of tracer uptake showing that it is directly proportional to the strength of the meridional overturning, i.e., an advectively dominated tracer uptake regime. It should be noted, however, that the two new diagnostics, basin averaged overturning streamfunction and the value of the streamfunction at 45°, are appropriate only for the domain used in this model and for equilibrium simulations.

Table 3. *Power relationship between two measures of the overturning streamfunction (OSF) and the vertical diffusivity; a similar scaling is done for the tracer uptake timescale (period)*

K_V	OSF (Peak) (Sv)	Δ ln (OSF)/ Δ ln (K_V)	OSF (45°) (Sv)	Δ ln (OSF)/ Δ ln (K_V)	Period (years)	Δ (ln T)/ Δ (ln K_V)
0.5	11.36	—	4.83	—	631	—
1.0	13.93	0.29	6.63	0.46	476	−0.41
2.0	17.19	0.30	9.52	0.52	341	−0.48

The horizontal diffusivity is held constant at $A_H = 1.0 \times 10^7$ cm^2/s for 3 cases.

3.2. *Tracer uptake for different temperature change scenarios*

The tracer uptake for different temperature change scenarios is examined in three ways. The first is to look at tracer uptake beginning with the equilibria circulation of four scenarios (standard, cold and two warms). The other two ways involve assessing the sensitivity of the uptake to periods of climatic change. This is done in two ways, the first is a sudden change in the surface temperature boundary condition and the second is a gradual change in the boundary condition ramped over one hundred years. All simulations begin with the standard climate and move toward one of the other three scenarios, similar to the approach used in Gough and Lin (1992).

3.2.1. Equilibrium uptake. In Table 2, the tracer uptake time for the three scenarios is presented. The two warming cases were essentially the same and are represented in the table together in the column labelled "b". The cold case is reported in column "c" while the regular or current climate is in column "a". The diagnostic used is the length of time to reach 95% of the equilibrium value of 10.0.

The variation in vertical diffusivity has the largest impact on the results for the values chosen in these experiments with the uptake timescale being reduced by a factor of close to two as illustrated by a comparison of cases 1 and 3. This is as expected as it has been well documented that larger values of vertical diffusivity intensifies the thermohaline circulation (as measured by the overturning streamfunction), thus leading to a more rapid sequestering of tracer to the lower levels by advection (Bryan, 1987; Gough and Welch, 1994). Larger values of the horizontal diffusivity also decreases the uptake timescale, although less so than the vertical diffusivity. This is consistent with the earlier analysis using the new diagnostics for meridional overturning.

Of the three factors, the choice of temperature scenario has the least impact. Consistently, though, the warmer case has a shorter uptake timescale than the regular climate and vice versa for the cooler case. These results are consistent with the previous results (Bryan and Spelman, 1985; Gough and Lin, 1992) in which warmer equilibria climates produced a more vigorous thermohaline circulation and the opposite for the cooler climates.

3.2.2. Sudden change to the new temperature scenario. In this set of experiments we begin with the equilibrium ocean flow generated under a surface temperature boundary condition that represents the current or "regular" climate. The boundary condition is then abruptly changed to the new conditions for a warmer or cooler scenario. Although the change in the surface temperature boundary condition is instantaneous, the ocean takes a period of 100s to 1000s of years to adjust to this change (Gough and Lin, 1992) depending on whether convection or diffusion dominates the adjustment period. As a benchmark, the current climate is also included (i.e., a scenario where no change is imposed).

In Fig. 3 the uptake of tracer is displayed for the four scenarios for 500 years after the change scenarios are imposed. The basin averaged tracer concentration is plotted as a function of time. The cooling scenario approaches the equilibrium value of 10.0 much more rapidly than the other scenarios. Within 50 years the average tracer value exceeds 5.0 while this takes 100 years for the current climate and over 300 years for the two warming scenarios. This asymmetry is consistent

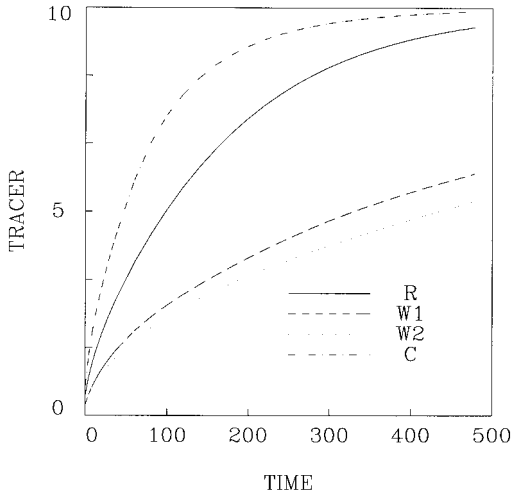

Fig. 3. Time evolution of tracer concentration for the four climate change scenarios for case 2 ($K_V = 1.0$ cm^2/s). *R* represents the standard climate. *C* represents a 3°C cooling everywhere. *W1* represents a 3°C warming everywhere. *W2* indicates a polar amplified warming.

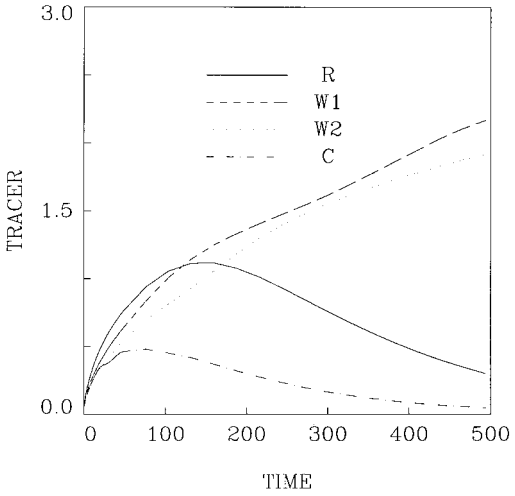

Fig. 4. Difference of time evolution of tracer variation for four climate scenarios between case 3 ($K_V =$ 2.0 cm^2/s) — case 2 ($K_v = 1.0$ cm^2/s). *R* represents the standard climate. *C* represents a 3°C cooling everywhere. *W1* represents a 3°C warming everywhere. *W2* indicates a polar amplified warming.

with the results of Gough and Lin (1992) where cooling produces an intensification of both convection and the thermohaline circulation and warming produces a shutdown of the thermohaline circulation and cessation of convection. The cooling experiment is convectively driven toward a new equilibrium while the warming experiments are diffusively driven and thus operate on vastly different time scales. Polar amplification of the warming produces qualitatively the same results with a minor reduction in tracer uptake time.

Fig. 4 illustrates the impact of varying the vertical diffusivity on the response to a sudden change. This figure depicts the difference between case 3 ($K_V = 2.0$ cm^2/s) and case 2 ($K_V = 1.0$ cm^2/s). For all the scenarios the higher vertical diffusivity sequesters tracer at a more rapid rate. For the cooling experiment this difference is relatively minor and drops essentially to zero by the end of the 500 year period. This is an indicator that convection rather than advection dominates the tracer uptake during the early part of the cooling experiment. The warming experiments in contrast have an increasing difference of over 2.0 tracer units at 500 years. The polar amplified warming produces only a small quantitative difference. Once again we see an asymmetric response where the value of the vertical diffusivity plays a more important role in the warming experiments thus indicating that the warming case is dominated by diffusion rather than convection or advection. An analysis of the horizontal diffusivity cases shows a similar response, approximately 20% of the vertical diffusivity variation.

These results show that the ocean's role as a buffer is mitigated during the transition to a warmer scenario potentially leading to a positive feedback in the climate system. They also show that model parameters such as vertical and horizontal diffusivity impact significantly on the timescale of adjustment processes. This is a crucial point for climate change impact assessment.

3.2.3. Ramped change. In these experiments the change in the upper surface temperature boundary condition is ramped in over 100 years. To illustrate the impact of the changes we present as a diagnostic the difference of tracer uptake between the ramped and corresponding sudden case. The absolute value of the difference is plotted. In the cooling experiment the sudden change uptake exceeds that of the ramped change due to the more rapid intensification of the flow and the reverse is true for the warming scenarios. Fig. 5 shows this plot for cases 2 and 3. For case 2, the ramped cooling

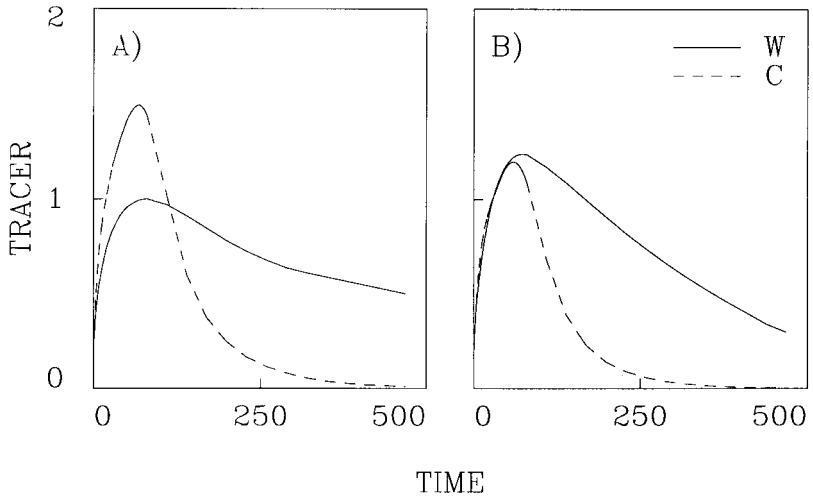

Fig. 5. Time evolution of the absolute difference between basin averaged tracer concentrations for corresponding sudden and ramped scenarios. *W* represents the 3°C warming scenario and *C* represents the 3°C cooling scenario for a) case 2 ($K_V = 1.0\ cm^2/s$) and b) case 3 ($K_V = 2.0\ cm^2/s$). For the cooling scenario the sudden case exceeds the ramped case and for the warming scenario the ramped case exceeds the sudden case in tracer concentration.

scenario takes up tracer less rapidly with the peak delay occurring at the end of the 100 year ramp in period. After this time, the ramped change case quickly approaches the sudden change uptake becoming virtually indistinguishable after 400 years.

The ramped warming experiment has a less pronounced departure from the corresponding sudden experiment initially but maintains a difference well past the 500-year tracer integration period. These results are consistent with the dynamical response of the model flow to surface warming and cooling (Gough and Lin, 1992). In the cooling scenarios, the ramped change delays and mitigates the intensification of the thermohaline circulation and convection, leading to the pronounced difference in the first 200 years. In the warming scenario, the ramped change delays the shutdown of both the thermohaline circulation and convective activity thus enabling more tracer to be sequestered particularly in the first hundred years. The very slow approach to the new equilibrium (compared to the cooling scenario) causes the continued difference between the warming ramped and sudden cases.

Case 3 (Fig. 5b) illustrates the impact of increasing the vertical diffusivity. The cooling scenario has a muted response compared to case 2 and the warming scenario has a slightly larger response compared to case 2. With a larger vertical diffusivity the initial equilibrium state is a more intense circulation (Table 2), thus the contrast between the intensified (cooling scenario) and initial states is less leading to a less pronounced difference between the ramped and sudden cooling experiments. Similarly for the warming experiment, there is a greater contrast between the initial state and the quiescent thermohaline circulation shutdown enabling a greater tracer uptake in the ramped case where the shutdown is both delayed and mitigated. Similar behaviour (not shown) is observed with increasing horizontal diffusivity.

4. Conclusions

In this work, we examine the rôle of model parameters, vertical and horizontal diffusivity, in the uptake of a passive tracer for several thermal change scenarios. An initial analysis is done on the current climate. It is found that the tracer uptake operates on a centennial timescale and therefore advection being the dominant uptake process. Vertical diffusivity thus plays a dominant role in determining the time scale of tracer uptake and horizontal diffusivity plays a smaller, but not

negligible, role. It is found, especially for the horizontal diffusivity analysis, that the use of the peak value of the overturning streamfunction is not the best indicator of overturning strength as was suggested by Winton (1996). A basin mean value and the value in the mid basin region are presented as measures and are consistent with the tracer uptake behaviour for the particular domain used.

The thermal change scenarios are assessed in three ways. First the tracer uptake for new equilibria is examined. Variations in the vertical and horizontal diffusivity produced much more significant changes to the model's flow than did variations in thermal forcing. However a different story emerged for the other two assessments, that is, the model's transient response to temperature change. This is done in two ways: the transient response to a sudden change in upper boundary condition and a ramped change (over 100 years) of the same net magnitude. In these results the cooling scenarios are the least sensitive to variations of model diffusivity. Surface cooling causes the densification of surface waters thus inducing convection which operates at a much shorter time scale than diffusion and advection. The warming cases, however, respond asymmetrically to the cooling cases and are very sensitive to variations in the vertical diffusivity causing uptake delays of the order of hundreds of years. This is a result of the collapse of the thermohaline circulation. The model thus responds on diffusive timescales rather than convective. The ramped experiments mitigated the extremes of the sudden experiments, i.e., less rapid tracer uptake for the cooling scenario and more rapid uptake for the warming scenario. This is a result of the less intense response in the cooling scenarios and the delay of thermohaline collapse in the warming scenarios consistent with behaviour found in Gough and Lin (1992). Larger diffusivities exaggerated the difference between ramped and sudden for the warming scenario and minimized the difference for the cooling scenario.

These experiments serve to illustrate some of the potential problems of using coarse resolution ocean models in coupled model climate simulations. The ocean response both for passive and active tracer variations is highly dependent on the tuning of the horizontal and vertical diffusivities. The convectively dominated climate cooling is somewhat immune to these variations but the more currently relevant warming scenarios are very much dependent on these parameters. This has important consequences in assessing the ocean's role as a thermal and geochemical buffer and its role in positive and negative feedbacks in the climate system, particularly on timescales of immediate human interest, decadal and centennial.

5. Acknowledgements

The authors wish to acknowledge financial support from the NSERC/AES Science subvention program. Helpful comments were provided by two anonymous reviewers.

REFERENCES

Bryan, F. 1987. Parameter sensitivity of primitive equation ocean general circulation models. *J. Phys. Oceanogr.* **17**, 970–985.

Bryan, K. 1969. A numerical method for the study of the circulation of the world ocean. *J. Comput. Phys.* **4**, 347–376.

Bryan, K. 1984. Accelerating convergence to equilibrium of ocean-climate models. *J. Phys. Oceanogr.* **14**, 666–673.

Bryan, K., Komro, F. G., and Rooth, C. 1984. The ocean's transient response to global surface temperature anomalies. In: *Climate processes and climate sensitivity*. Maurice Ewing, vol. 5, J. E. Hansen and T. Takahashi (eds.). Am. Geophys. Union, Washington, D. C., pp. 29–38.

Bryan, K. and R. Spelman, 1985. The ocean's response to a CO_2 induced warming. *J. Geophys. Res.* **90**, 11 679–11 688.

Cox, M. 1984. A primitive equation, three dimensional model of the ocean. *GFDL Ocean Tech. Report No.* **1**. Princeton, New Jersey.

Danabasoglu, G., McWilliams, J., and Gent, P. 1994. The role of mesoscale tracer transports in the general circulation of the oceans. *Science* **254**, 1123–1126.

England, M. 1995. Using chlorofluorocarbons to assess ocean climate models. *Geophys. Res. Lett.* **22**, 3051–3054.

Gent, P., Willebrand, J., McDougall, T., and McWilliams, J. 1995. Parameterizing eddy-induced transports in an ocean general circulation models. *J. Phys. Oceanogr.* **25**, 463–474.

Gough, W. and Lin, C. 1992. The response of an ocean

general circulation model to long time-scale surface temperature anomalies. *Atmos.-Ocean* **30**, 653–674.

Gough, W. and Welch, W. 1994. Parameter space exploration of an ocean general circulation model using an isopycnal mixing parameterization. *J. Mar. Res.* **52**, 773–796.

Gough, W. and Lin, C. 1995. Isopycnal mixing and the Veronis effect in an ocean general circulation model. *J. Mar. Res.* **53**, 189–199.

Gough, W. 1997. Convective adjustment and isopycnal mixing in an ocean general circulation model. *Atmos. Ocean*, in press.

Haney, R. 1971. Surface thermal boundary conditions for ocean circulation models. *J. Phys. Oceanogr.* **1**, 241–248.

Houghton, J., Jenkins, G. and Ephraums, J. (eds.). 1990. *Climate change*. The IPCC scientific assessment. Cambridge University Press. Cambridge, UK, 365 pp.

Kattenberg, A., Giorgi, F., Grassl, H., Meehl, G., Mitchell, J., Stouffer, R., Tokiada, T., Weaver, A. and Wigley, T. 1996. *Climate models — predictions of future climate*. In: Climate change 1995: The science of climate change. Cambridge University Press, Cambridge, UK, 549 pp.

Ledwell, J., Watson, A. and Law, S. 1993. Evidence for slow mixing across the pycnocline from an open ocean tracer release experiment. *Nature* **364**, 701–703.

Levitus, S. 1982. *Climatological atlas of the world oceans*. NOAA Prof. Paper 13, Washington, D. C.

McDougall, T. and Church, J. 1985. Pitfalls with numerical representation of isopycnal and diapycnal mixing. *J. Phys. Oceanogr.* **16**, 196–199.

Najjar, R. 1992. Marine biogeochemistry. In: *Climate system modelling*, Trenberth, K. (ed.). Cambridge University Press, Cambridge, pp. 241–282.

Pacanowski, R., K. Dixon and A. Rosati, 1991. The GFDL modular ocean model user guide, GFDL *Group Technical Report* #**2**, 44 p.

Robitaille, D. and Weaver, A. 1995. Validation of subgrid scale mixing schemes using CFCs in a global ocean general circulation model. *Geophys. Res. Lett.* **22**, 2917–2920.

Sarmiento, J. 1983. A simulation of bomb tritium entry into the Atlantic Ocean. *J. Phys. Oceanogr.* **13**, 1924–1939.

Toggweiler, R., Dixon, K., and Bryan, K. 1989. Simulations of radiocarbon in a coarse-resolution world ocean model. (2) Distribution of bomb-produced carbon 14. *J. Geophys. Res.* **94**, 8243–8264.

Veronis, G. 1975. *The rôle of models in tracer studies in numerical models of ocean circulation*. National Academy of Sciences, 133–146.

Winton, M. 1996. On the role of horizontal boundaries in parameter sensitivity and decadal-scale variability of coarse-resolution ocean general circulation model. *J. Phys. Oceanogr.* **26**, 289–304.